PHYSICS

# Aggregation of solutes in bosonic versus fermionic quantum fluids

**Alexandra J. Feinberg[1], Deepak Verma[1,2], Sean M.O. O'Connell-Lopez[1,3], Swetha Erukala[1], Rico Mayro P. Tanyag[1,4], Weiwu Pang[5], Catherine A. Saladrigas[6,7], Benjamin W. Toulson[6], Mario Borgwardt[6], Niranjan Shivaram[8,9], Ming-Fu Lin[8], Andre Al Haddad[10], Wolfgang Jäger[11], Christoph Bostedt[10,12], Peter Walter[8], Oliver Gessner[6]*, Andrey F. Vilesov[1,13]***



**Quantum fluid droplets made of helium-3 ($^3$He) or helium-4 ($^4$He) isotopes have long been considered as ideal cryogenic nanolabs, enabling unique ultracold chemistry and spectroscopy applications. The droplets were believed to provide a homogeneous environment in which dopant atoms and molecules could move and react almost as in free space but at temperatures close to absolute zero. Here, we report ultrafast x-ray diffraction experiments on xenon-doped $^3$He and $^4$He nanodroplets, demonstrating that the unavoidable rotational excitation of isolated droplets leads to highly anisotropic and inhomogeneous interactions between the host matrix and enclosed dopants. Superfluid $^4$He droplets are laced with quantum vortices that trap the embedded particles, leading to the formation of filament-shaped clusters. In comparison, dopants in $^3$He droplets gather in diffuse, ring-shaped structures along the equator. The shapes of droplets carrying filaments or rings are direct evidence that rotational excitation is the root cause for the inhomogeneous dopant distributions.**

## INTRODUCTION

Quantum fluid nanodroplets made of liquid helium are exceptional hosts for isolated cryogenic matrix applications (*1*–*5*). The droplets readily pick up atoms and molecules (*6*), providing unique opportunities to study the formation of molecular complexes close to absolute zero temperatures. Additionally, the large degree of quantum mechanical delocalization in helium enables unique matrix configurations around the dopants, giving rise to a perfectly tailored void around each particular molecule (*3*).

Previously, small $^4$He droplets containing less than ~$10^4$ atoms, roughly 10 nm in diameter, were used for the spectroscopic interrogation of molecules and molecular complexes at a temperature of about 0.4 K (*1*–*5*). It was long believed that, unlike immobilized dopant molecules in solid matrices, dopants in helium nanodroplets could move unhindered and stochastically (*3*, *7*). Recent ultrafast x-ray coherent diffractive imaging (CDI) experiments with large xenon-doped superfluid $^4$He droplets, a few hundreds of nanometers in diameter, have revealed a markedly different scenario (*8*–*10*). Instead of forming the once proposed ramified entities (*7*), dopant atoms were found to aggregate in arrays of elongated filament-shaped clusters (*9*, *10*). This effect was assigned to inhomogeneities within the droplets due to the presence of quantum vortices, which attract dopant particles (*11*–*14*). The vortices were found to originate from an unavoidable rotational excitation of free helium droplets in the beam (*8*, *15*–*17*), implying that the superfluid nature of $^4$He enhances the inhomogeneity of matrix-dopant interactions.

To provide unequivocal proof for the link between inhomogeneous dopant distributions, the superfluid nature of $^4$He droplets, and their rotational excitation, comparative measurements are required on fermionic $^3$He and superfluid, bosonic $^4$He droplets. Note that $^3$He can also enter the superfluid state, but it does so at much lower temperatures ($T$ ~ 1 mK) (*18*, *19*) than are present in our experiment ($T$ ~ 0.15 K) (*20*). Thus, $^3$He droplets act as a normal fluid under our experimental conditions and serve as a reference droplet devoid of vortices. Here, we present a comparative study on the aggregation of xenon atoms in submicrometer-sized $^3$He and $^4$He droplets. Our results show that dopants are subject to a high degree of spatial confinement within both $^3$He and $^4$He nanodroplets, with each isotope giving rise to markedly different dopant morphologies.

## RESULTS

Figures 1 and 2 show plane projections of $^4$He and $^3$He droplets, respectively, with their reconstructed xenon dopant density distributions for a variety of representative droplets (*10*). The details on the reconstruction of density from diffraction images and the description of the results are described in Materials and Methods. The $^3$He and $^4$He droplets studied in this work have similar diameters in the range of 400 to 600 nm, containing on the order of $10^9$ helium atoms per droplet. Corresponding diffraction images are presented in the Supplementary Materials.

Most outlines are ellipses, consistent with spheroidal, rotating droplets (*8*, *15*, *17*, *21*, *22*). In previous studies, it was found that a cryogenic fluid expansion into vacuum readily produces rotating $^4$He and $^3$He droplets (*15*, *17*). It was also found that droplets of different isotopes have very similar average aspect ratios of about 1.05 for

[1]Department of Chemistry, University of Southern California, Los Angeles, CA 90089, USA. [2]RA3, Intel Corporation, Ronler Acres, 2501 NE Century Blvd, Hillsboro, OR 97124, USA. [3]Rosenstiel School of Marine and Atmospheric Sciences, University of Miami, 4600 Rickenbacker Cswy., Miami, FL 33149, USA. [4]Department of Chemistry, Aarhus University, 8000 Aarhus C, Denmark. [5]Viterbi School of Engineering, University of Southern California, Los Angeles, CA 90089, USA. [6]Chemical Sciences Division, Lawrence Berkeley National Laboratory, Berkeley, CA 94720, USA. [7]Department of Chemistry, University of California, Berkeley, Berkeley, CA 94720, USA. [8]SLAC National Accelerator Laboratory, 2575 Sand Hill Road, Menlo Park, CA 94025, USA. [9]Department of Physics and Astronomy, Purdue University, West Lafayette, IN 47907, USA. [10]Laboratory for Femtochemistry (LSF), Paul Scherrer Institut, Forschungsstrasse 111, 5232 Villigen-PSI, Switzerland. [11]Department of Chemistry, University of Alberta, Edmonton, Alberta T6G 2G2, Canada. [12]LUXS Laboratory for Ultrafast X-ray Sciences, Institute for Chemical Sciences and Engineering, École Polytechnique Fédérale de Lausanne (EPFL), CH-1015 Lausanne, Switzerland. [13]Department of Physics and Astronomy, University of Southern California, Los Angeles, CA 90089, USA.
*Corresponding author. Email: ogessner@lbl.gov (O.G.); vilesov@usc.edu (A.F.V.)

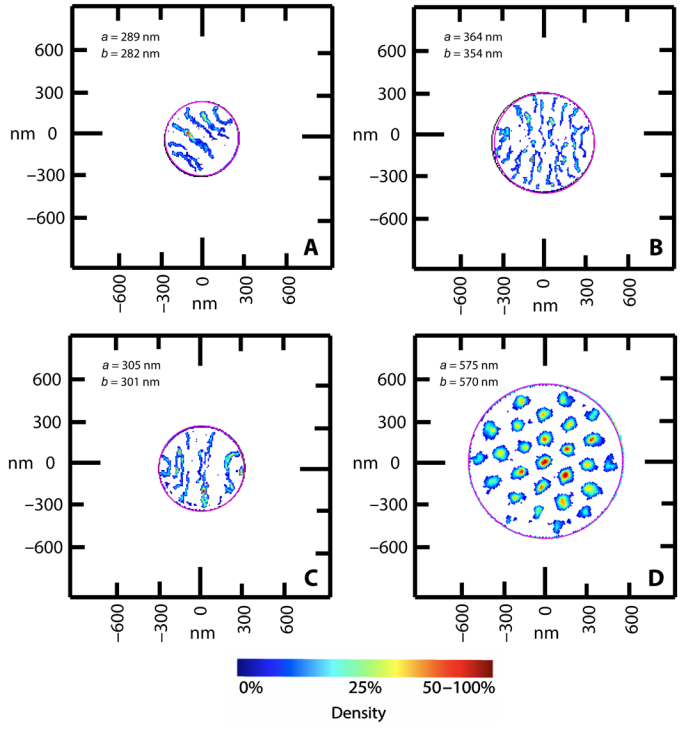


**Fig. 1. Aggregation in $^4$He droplets.** Outlines of the droplets are shown in black, and the xenon dopant density distributions are shown in blue-red. (**A** to **D**) Results for four different representative superfluid $^4$He droplets. The values *a* and *b* of the long and short half axes, respectively, of the droplet's projection onto the detector plane are given in each panel. For visualization, circular contours (magenta) have been superimposed on the droplets with a radius equal to that of the minor half axis. Closer inspection reveals slightly elliptical distortions, most prominent in droplet *b*.

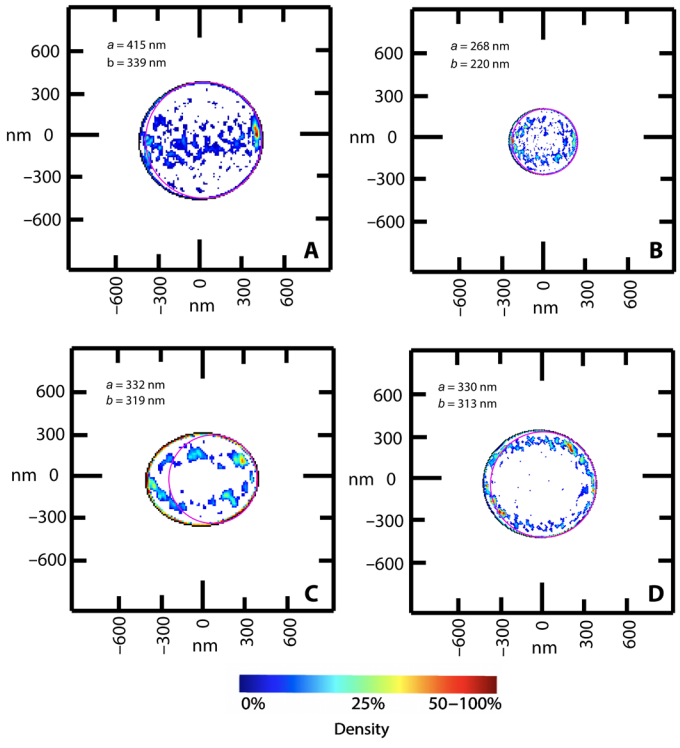


**Fig. 2. Aggregation in $^3$He droplets.** Outlines of the droplets are shown in black, and the xenon dopant density distributions are shown in blue-red. (**A** to **D**) Results for four different representative normal fluid $^3$He droplets. The values of the long and short half axes of the droplet's projection onto the detector plane are given in each panel. For visualization, circular contours (magenta) have been superimposed on the droplets with a radius equal to that of the minor half axis. Note the partly substantial elliptical distortions of the droplet outlines.

their projections on the detector plane (*17*). We hypothesized that during the passage of fluid helium through the nozzle, the fluid interacts with the nozzle channel walls and acquires vorticity, which is eventually transferred to the droplets. Figure 1 illustrates several $^4$He droplets and their dopant density distributions. As previously demonstrated (*9*, *10*), the droplets contain several strongly aligned tracks of high density, which are assigned to xenon atoms aggregating inside the cores of quantum vortices. Vortices in Fig. 1 (A to C) are viewed from the side, while vortices in Fig. 1D point toward the viewer, revealing their arrangement in a triangular lattice configuration that closely resembles the arrangements of vortices observed in rotating cylinders filled with $^4$He (*11*, *14*) and in trapped Bose-Einstein condensates (*23*).

Results are markedly different for xenon-doped $^3$He droplets, as illustrated in Fig. 2. Here, xenon clusters appear either as a stripe (Fig. 2A) or as elliptical structures (Fig. 2, B to D) that are aligned along the droplets' long axes. In Fig. 2D, xenon atoms form a loose ring of clusters on the droplet's periphery. During the imaging event, the x-ray beam forms an arbitrary angle with the droplet's figure axis; therefore, their real aspect ratios are larger than indicated by their outlines in Figs. 1 and 2, which correspond to projections of the droplets on the detector plane. The images are characterized by the two half axes of the droplet's projection, referred to as *a* and *b* ($a > b$), corresponding to a projection aspect ratio, $AR = a/b$. The formation of rings is observed in $^3$He droplets having $AR = 1.04$ to $AR = 1.2$ (Fig. 2).

A smaller amount of data was obtained for $^4$He droplets during the same experimental run. Most of the intense, reconstructable $^4$He images have a small aspect ratio ($AR < 1.05$). However, the results obtained during our previous studies show the formation of vortex arrays in droplets having up to $AR = 2.4$ (*9*). Thus, we observe confinement of dopants across a wide range of aspect ratios.

The lower boundaries for the droplet's angular velocity, estimated from their aspect ratios (*17*), are $\approx 1.1 \times 10^7$ and $\approx 1.5 \times 10^6$ rad/s for the droplets in Fig. 2 (C and D, respectively). In comparison, the angular velocity of the $^4$He droplet in Fig. 1D is estimated to be $\approx 1.7 \times 10^6$ rad/s based on the areal density of the vortices and using the Feynman relation (*24*). The pronounced alignment of the xenon cluster contours along the long axes of the $^3$He droplets strongly suggests that the xenon dopants form rings in the droplets' equatorial planes, with their apparent ellipticity determined by the viewing angle.

Statistically, there is a large difference between the shapes of the xenon density distributions within $^3$He and $^4$He droplets. No aligned filaments, which are characteristic for superfluid $^4$He droplets, are observed in $^3$He droplets. Instead, these fermionic droplets contain diffuse ring-shaped structures. It is unlikely that the ring structures could be attributed to any impurities. The $^3$He gas used was 99.9% pure with the remaining 0.1% being mostly $^4$He. Considering that $^4$He's solubility in $^3$He is ~0.1% at 0.15 K, any residual $^4$He will likely be dissolved

in the $^3$He droplets. Even if any pockets of a $^4$He-rich phase were formed, they would be too small to give rise to any measurable effects in the diffraction patterns (*17*).

## DISCUSSION

It is immediately apparent from the dopant density distributions presented in Figs. 1 and 2 that helium nanodroplets are not homogenous nanolabs. In both isotopes, dopants are subject to unavoidable, high degrees of spatial confinement due to the droplets' rotation. In $^4$He, vortex-bound xenon is aligned along the minor axis of the droplets, as discussed in more detail elsewhere (*9*), whereas in $^3$He, xenon is confined along the droplet's equator. The direct relation between the direction of the $^3$He droplet's long axis and the concentration of xenon along the equator is visually apparent in Fig. 2. The distorted shapes of $^3$He and $^4$He droplets carrying dopant rings or filaments, respectively, are direct evidence that rotational excitation is the root cause for the inhomogeneous dopant distributions.

Clusters formed in fermionic $^3$He and bosonic $^4$He droplets exhibit distinctly different structures. Thus, nuclear spin, which has no impact on any property of ordinary solvents at higher temperatures, plays a crucial role in determining the aggregation dynamics of dopants at low temperatures. We propose that the mechanism for cluster formation in large helium droplets differs between superfluid $^4$He and normal fluid $^3$He. In $^4$He, single xenon atoms are picked up by the droplet, rapidly thermalize, and begin to move freely within the confines of the droplet's boundaries (*3*). Atoms form clusters upon collisions. At the same time, xenon atoms and small clusters are attracted to the cores of the vortices by hydrodynamic forces (*11*–*14*) and form large, filament-shaped aggregates. In comparison, in a $^3$He droplet devoid of vortices, xenon clusters will likely form throughout the entire droplet volume, followed by coalescence into larger globular cluster-cluster aggregates. However, because of the high viscosity of $^3$He droplets, dopants assume the same angular velocity as the host and congregate close to the droplet's surface along the equator, i.e., in a plane perpendicular to the direction of the angular momentum. The positions of the dopants are defined by a balance between centrifugal forces and the dopants' solvation potential (*25*). In principle, similar ring-shaped clusters are expected to be formed in classical rotating droplets (e.g., water droplets with heavy colloidal clusters); however, we are unaware of such studies. The ring-shaped xenon structures appear to consist of separate, small (~50 nm) clusters, some of which exhibit branched shapes. The structures are likely defined during their formation and remain frozen at the low droplet temperature. The clusters appear to be separated and do not collapse into larger cluster-cluster aggregates, indicating that some mechanism stabilizes the porous network. Previously, it was proposed that some weakly interacting atoms (e.g., magnesium) may form a so-called foam (*26*–*28*), where the atoms stay at subnanometer distance because of the shell of surrounding helium atoms. Whereas x-ray diffraction could be a useful technique for identifying the foam state, the resolution of current small-angle soft x-ray scatting experiments of about 20 nm is insufficient to resolve spatial features on this level of detail. It is conceivable that the clusters have some interlinks that are too thin to be detected. The smallest compact cluster that can be detected in this work contains ~1000 xenon atoms and will appear in an image as approximately 3 × 3 pixels in size. This limit is set by the threshold of the phase retrieval algorithm and the spatial resolution of the measurements (*10*). Future high-resolution experiments may shed more light on the atomic structure of aggregates obtained at temperatures close to 0 K.

The few 100-nm-sized droplets in this study, which are produced from fragmentation of the supercritical fluid in the cryogenic nozzle, are marked by large angular velocities of $10^6$ to $10^7$ rad/s. This contrasts with the results for small droplets of few nanometers in diameter produced via aggregation of helium atoms. For example, extensive spectroscopy experiments on molecules in small (a few nanometers) $^4$He droplets did not indicate any presence of quantum vortices (*29*). On the other hand, centrifugal displacement of molecules from the droplet's center was discussed (*30*). The locations of molecules in small droplets could not be identified in the previous spectroscopy studies on either $^3$He or $^4$He, and the dopants are often assumed to reside close to the droplet's center (*3*, *4*). We observe that vortices in $^4$He are typically separated by distances of 100 to 200 nm; thus, smaller droplets of 150 to 200 nm in diameter may contain just a single vortex. This shows that smaller $^4$He droplets between 50 and 100 nm in diameter may be devoid of vortices. Some other techniques of producing helium droplets at small velocity, other than in a molecular beam, may be considered to produce $^4$He droplets devoid of vortices.

## MATERIALS AND METHODS

### Production and doping of $^3$He and $^4$He droplets

Large nanodroplets are produced by expanding pressurized $^4$He (99.9999%) or $^3$He (99.9%) fluid through a cryogenic nozzle into vacuum with a stagnation pressure of $P_0$ = 20 bar and a nozzle temperature $T_0$ = 5 K (*3*, *8*, *17*, *31*). Under these expansion conditions, droplets with average radii of ~160 and ~350 nm are produced for $^3$He and $^4$He, respectively (*17*). Once in vacuum, the droplets evaporatively cool to respective temperatures of 0.15 K for $^3$He (*20*) and 0.38 K for $^4$He (*32*). The droplets exit the source chamber with an average velocity of about 190 m/s for $^3$He and 160 m/s for $^4$He and subsequently enter the pickup chamber, which is filled with xenon (99.9%) gas. The droplets collide with and pick up several xenon atoms, evaporating off ~750 $^3$He or ~250 $^4$He atoms with the pickup of each xenon atom. The amount of xenon added is measured by monitoring the relative depletion of the mass $M$ = 8 signal for $^4$He (or $M$ = 6 for $^3$He), representative of $He_2^+$ ions, in a quadrupole mass spectrometer installed in the terminal vacuum chamber (*8*). The droplets in Figs. 1 and 2 contain ~$10^9$ helium atoms and between $10^5$ and $10^6$ xenon atoms. The $^3$He gas was collected, purified, and recirculated by a gas-recycling system as described elsewhere (*17*).

### X-ray diffraction from Xe-doped $^3$He and $^4$He droplets

Xenon-doped droplets are irradiated by a focused x-ray free-electron laser (XFEL) beam operated at 1.5 keV ($\lambda$ = 0.826 nm) (*8*). The FEL beam consists of ultrashort x-ray pulses, containing up to ~$10^{12}$ photons/pulse, with a repetition rate of 120 Hz, a pulse energy of 1.5 mJ, and a pulse duration of ~100 fs (full width at half maximum). The small pulse length and large number of photons per pulse enable the instantaneous capture of the shapes of individual droplets. Diffraction images are recorded with a *pn*-charge-coupled device detector containing 1024 × 1024 pixels, each 75 μm by 75 μm in size, which is centered along the FEL beam axis ~735 mm downstream from the interaction point. The detector consists of two separate panels (1024 × 512 pixels each) located closely above and below the x-ray

beam. Both panels have a central, rectangular cutout to accommodate the primary x-ray beam.

### Density retrieval, size, and shape determination

The diffraction patterns are recorded at small scattering angles and thus predominantly contain information on the column density of the droplets in the direction perpendicular to the detector plane. During the measurements, roughly 550 diffraction patterns from xeno-doped $^3$He nanodroplets were obtained, whereas 200 patterns were obtained as a reference for xeno-doped $^4$He droplets. Among them, only the brightest images containing more than ~$10^5$ detected photons were selected for reconstruction (*10*). Four representative hits were selected from the $^4$He data, whereas four hits were selected from the $^3$He data. Using an iterative phase retrieval algorithm, termed droplet (DCDI), the density profiles of the xenon clusters inside the droplets are reconstructed, and the sizes and shapes are determined (*10*). Similar $^3$He and $^4$He droplet reconstructions are compared on the basis of size, aspect ratio, and overall number of photons detected.

Helium droplet shapes are described by the distances between the center and the surface in three mutually perpendicular directions: $A > B > C$. The observed diffraction patterns do not provide direct access to the actual values of $A$, $B$, and $C$, because of the droplets' unknown orientations with respect to the x-ray beam. Instead, the images are characterized by the two half axes of the projection of a droplet onto the detector plane, which are referred to as $a$ and $b$ ($a > b$), corresponding to a projection aspect ratio, $AR = a/b$. The majority (99%) of helium droplets are close to spherical with $AR < 1.4$ corresponding to oblate, axially symmetric shapes. For those shapes with $AR < 1.4$, the average aspect ratios for each isotope are similar, with $AR = 1.049 \pm 0.003$ for $^3$He and $1.059 \pm 0.005$ for $^4$He (*17*).

## SUPPLEMENTARY MATERIALS

Supplementary material for this article is available at https://science.org/doi/10.1126/sciadv.abk2247

## REFERENCES AND NOTES


1. M. Hartmann, R. E. Miller, J. P. Toennies, A. F. Vilesov, High-resolution molecular spectroscopy of van der Waals clusters in liquid helium droplets. *Science* **272**, 1631–1634 (1996).
2. K. K. Lehmann, G. Scoles, The ultimate spectroscopic matrix? *Science* **279**, 2065–2066 (1998).
3. J. P. Toennies, A. F. Vilesov, Superfluid helium droplets: A uniquely cold nanomatrix for molecules and molecular complexes. *Angew. Chem. Int. Ed. Engl.* **43**, 2622–2648 (2004).
4. M. Y. Choi, G. E. Douberly, T. M. Falconer, W. K. Lewis, C. M. Lindsay, J. M. Merritt, P. L. Stiles, R. E. Miller, Infrared spectroscopy of helium nanodroplets: Novel methods for physics and chemistry. *Int. Rev. Phys. Chem.* **25**, 15–75 (2006).
5. A. Mauracher, O. Echt, A. M. Ellis, S. Yang, D. K. Bohme, J. Postler, A. Kaiser, S. Denifl, P. Scheier, Cold physics and chemistry: Collisions, ionization and reactions inside helium nanodroplets close to zero K. *Phys. Rep.* **751**, 1–90 (2018).
6. M. Lewerenz, B. Schilling, J. P. Toennies, Successive capture and coagulation of atoms and molecules to small clusters in large liquid helium clusters. *J. Chem. Phys.* **102**, 8191–8207 (1995).
7. S. G. Alves, A. F. Vilesov, S. C. Ferreria Jr., Effects of the mean free path and relaxation in a model for the aggregation of particles in superfluid media. *J. Chem. Phys.* **130**, 244506 (2009).
8. L. F. Gomez, K. R. Ferguson, J. P. Cryan, C. Bacellar, R. M. P. Tanyag, C. Jones, S. Schorb, D. Anielski, A. Belkacem, C. Bernando, R. Boll, J. Bozek, S. Carron, G. Chen, T. Delmas, L. Englert, S. W. Epp, B. Erk, L. Foucar, R. Hartmann, A. Hexemer, M. Huth, J. Kwok, S. R. Leone, J. H. S. Ma, F. R. N. C. Maia, E. Malmerberg, S. Marchesini, D. M. Neumark, B. Poon, J. Prell, D. Rolles, B. Rudek, A. Rudenko, M. Seifrid, K. R. Siefermann, F. P. Sturm, M. Swiggers, J. Ullrich, F. Weise, P. Zwart, C. Bostedt, O. Gessner, A. F. Vilesov, Shapes and vorticities of superfluid helium nanodroplets. *Science* **345**, 906–909 (2014).
9. S. M. O. O'Connell, R. M. P. Tanyag, D. Verma, C. Bernando, W. Pang, C. Bacellar, C. A. Saladrigas, J. Mahl, B. W. Toulson, Y. Kumagai, P. Walter, F. Ancilotto, M. Barranco, M. Pi, C. Bostedt, O. Gessner, A. F. Vilesov, Angular momentum in rotating superfluid droplets. *Phys. Rev. Lett.* **124**, 215301 (2020).
10. R. M. P. Tanyag, C. Bernando, C. F. Jones, C. Bacellar, K. R. Ferguson, D. Anielski, R. Boll, S. Carron, J. P. Cryan, L. Englert, S. W. Epp, B. Erk, L. Foucar, L. F. Gomez, R. Hartmann, D. M. Neumark, D. Rolles, B. Rudek, A. Rudenko, K. R. Siefermann, J. Ullrich, F. Weise, C. Bostedt, O. Gessner, A. F. Vilesov, Communication: X-ray coherent diffractive imaging by immersion in nanodroplets. *Struct. Dyn.* **2**, 051102 (2015).
11. G. P. Bewley, D. P. Lanthrop, K. R. Sreenivasan, Visualization of quantized vortices. *Nature* **441**, 588 (2006).
12. F. Coppens, F. Ancilotto, M. Barranco, N. Halberstat, M. Pi, Dynamics of impurity clustering in superfluid $^4$He nanodroplets. *Phys. Chem. Chem. Phys.* **31**, 17423–17432 (2019).
13. W. Guo, M. La Manita, D. Lathrop, S. W. Van Sciver, Visualization of two-fluid flows of superfluid helium-4. *Proc. Natl. Acad. Sci. U.S.A.* **111**, 4653–4658 (2014).
14. E. J. Yarmchuck, M. V. J. Gordon, R. E. Packard, Observation of stationary vortex arrays in rotating superfluid-helium. *Phys. Rev. Lett.* **43**, 214–217 (1979).
15. B. Langbehn, K. Sander, Y. Ovcharenko, C. Peltz, A. Clark, M. Coreno, R. Cucini, M. Drabbels, P. Finetti, M. di Fraia, L. Giannessi, C. Grazioli, D. Iablonskyi, A. C. LaForge, T. Nishiyama, V. Oliver Álvarez de Lara, P. Piseri, O. Plekan, K. Ueda, J. Zimmermann, K. C. Prince, F. Stienkemeier, C. Callegari, T. Fennel, D. Rupp, T. Möller, Three-dimensional shapes of spinning helium nanodroplets. *Phys. Rev. Lett.* **121**, 255301 (2018).
16. D. Rupp, N. Monserud, B. Langbehn, M. Sauppe, J. Zimmermann, Y. Ovcharenko, T. Möller, F. Frassetto, L. Poletto, A. Trabattoni, F. Calegari, M. Nisoli, K. Sander, C. Peltz, M. J. Vrakking, T. Fennel, A. Rouzée, Coherent diffractive imaging of single helium nanodroplets with a high harmonic generation source. *Nat. Commun.* **8**, 493 (2017).
17. D. Verma, S. M. O. O'Connell, A. J. Feinberg, S. Erukala, R. M. P. Tanyag, C. Bernando, W. Pang, C. A. Saladrigas, B. W. Toulson, M. Borgwardt, N. Shivaram, M. F. Lin, A. al Haddad, W. Jäger, C. Bostedt, P. Walter, O. Gessner, A. F. Vilesov, Shapes of rotating normal fluid $^3$He versus superfluid $^4$He droplets in molecular beams. *Phys. Rev. B* **102**, 014504 (2020).
18. E. R. Dobbs, *Helium Three* (Oxford Univ. Press, 2000).
19. D. R. Tilley, J. Tilley, *Superfluidity and Superconductivity* (Institute of Physics Publishing, 1990).
20. B. G. Sartakov, J. P. Toennies, A. F. Vilesov, Infrared spectroscopy of carbonyl sulfide inside a pure 3He droplet. *J. Chem. Phys.* **136**, 134316 (2012).
21. F. Ancilotto, M. Barranco, M. Pi, Spinning superfluid $^4$He nanodroplets. *Phys. Rev. B* **97**, 184515 (2018).
22. M. Pi, F. Ancilotto, M. Barranco, Rotating $^3$He droplets. *J. Chem. Phys.* **152**, 184111 (2020).
23. J. R. Abo-Shaeer, C. Raman, J. M. Vogels, W. Ketterle, Observation of vortex lattices in Bose-Einstein condensates. *Science* **292**, 476–479 (2001).
24. R. P. Feynman, *Application of Quantum Mechanics to Liquid Helium* (North Holland Publishing Company, 1955), vol. 2, pp. 17–53.
25. C. Bernando, A. F. Vilesov, Kinematics of the doped quantum vortices in superfluid helium droplets. *J. Low. Temp. Phys.* **191**, 242–256 (2018).
26. E. B. Gordon, Impurity condensation in liquid and solid helium. *Low Temp. Phys.* **30**, 756–762 (2004).
27. S. Gode, R. Irsig, J. Tiggesbaumker, K. H. Meiwes-Broer, Time-resolved studies on the collapse of magnesium atom foam in helium nanodroplets. *New J. Phys.* **15**, 015026 (2013).
28. J. Eloranta, Theoretical study of quantum gel formation in superfluid $^4$He. *J. Low Temp. Phys.* **162**, 718–723 (2011).
29. K. K. Lehmann, R. Schmied, Energetics and possible formation and decay mechanisms of vortices in helium nanodroplets. *Phys. Rev. B* **68**, 224520 (2003).
30. K. K. Lehmann, Potential of a neutral impurity in a large 4He cluster. *Mol. Phys.* **97**, 645–666 (1999).
31. O. Bünermann, M. Dvorak, F. Stienkemeier, A. Hernando, R. Mayol, M. Pi, M. Barranco, F. Ancilotto, Calcium atoms attached to mixed helium droplets: A probe for the $^3$He-$^4$He interface. *Phys. Rev. B* **79**, 214511 (2009).
32. S. Grebenev, J. P. Toennies, A. F. Vilesov, Superfluidity within a small helium-4 cluster: The microscopic Andronikashvili experiment. *Science* **279**, 2083–2086 (1998).


**Acknowledgments:** We acknowledge the Natural Sciences and Engineering Research Council of Canada. **Funding:** This material is based on work supported by the NSF under grant no. DMR-1701077 and CHE-1664990 (to A.F.V.). C.A.S., B.W.T., M.B., and O.G. are supported by the Atomic, Molecular, and Optical Sciences Program of the U.S. Department of Energy, Office of Science, Office of Basic Energy Sciences, Chemical Sciences, Geosciences and Biosciences Division, through contract no. DE-AC02-05CH11231. M.B. acknowledges support by the Alexander von Humboldt foundation. Portions of this research were carried out at the Linac Coherent Light Source (LCLS) at the SLAC National Accelerator Laboratory. SLAC National

Accelerator Laboratory is supported by the U.S. Department of Energy, Office of Science, Office of Basic Energy Sciences under contract no. DE-AC02-76SF00515. **Author contributions:** A.F.V., O.G., and C.B. conceived the experiment. A.J.F., D.V., S.M.O.O., S.E., C.A.S., B.W.T., M.B., N.S., M.-F.L., P.W., O.G., and A.F.V. prepared and carried out the experiment. A.J.F., D.V., and A.F.V. performed the data analysis. R.M.P.T. and W.P. contributed to the development of the phase retrieval algorithm and took part in the preliminary experiments. A.A.H. and C.B. provided support for online data analysis. S.M.O.O., W.J., and A.F.V. constructed the recycling apparatus for $^3$He gas. A.J.F., O.G., and A.F.V. wrote the manuscript. **Competing interests:** The authors declare that they have no competing interests. **Data and materials availability:** All data needed to evaluate the conclusions in the paper are present in the paper and/or the Supplementary Materials.

Submitted 29 June 2021
Accepted 22 October 2021
Published 10 December 2021
10.1126/sciadv.abk2247